https://doi.org/10.1016/j.jobe.2021.102818

Analytical investigation on the load-moment interaction behavior of the FRP reinforced geopolymer concrete filled FRP tube circular columns

Junaid Ahmad[a,b], Shehroze Ali[c], Tao Yu[d], M. Neaz Sheikh[e], Muhammad N.S. Hadi[f,*]

[a]*PhD Candidate, School of Civil, Mining and Environmental Engineering, University of Wollongong, NSW 2522, Australia. Email: ja608@uowmail.edu.au (ORCID: 0000-0002-6139-6833)*

[b]*Lecturer (presently on leave), NUST Institute of Civil Engineering (NICE), National University of Sciences and Technology (NUST), Islamabad, Pakistan.*

[c]*PhD Candidate, School of Civil, Mining and Environmental Engineering, University of Wollongong, NSW 2522, Australia. Email: sa217@uowmail.edu.au (ORCID: 0000-0002-8239-5135)*

[d]*Professor, Department of Civil and Environmental Engineering, The Hong Kong Polytechnic University, Hung Hom, Kowloon, Hong Kong, China. Email: tao-cee.yu@polyu.edu.hk (ORCID: 0000-0003-4167-4127)*

[e]*Associate Professor, School of Civil, Mining and Environmental Engineering, University of Wollongong, NSW 2522, Australia. Email: msheikh@uow.edu.au (ORCID: 0000-0003-0110-5034)*

[f]*Associate Professor, School of Civil, Mining and Environmental Engineering, University of Wollongong, NSW 2522, Australia. Email: mhadi@uow.edu.au (ORCID: 0000-0002-6490-889X)*

**Corresponding Author*

Abstract

In this study, the load moment (*P-M*) interaction behavior of geopolymer concrete (GPC) filled fiber reinforced polymer (FRP) tube circular columns internally reinforced with FRP bars was analytically investigated. An analytical model for the *P-M* interaction behavior of the column was developed and validated against the experimental investigation results. The analytical model incorporates the confined GPC strength and the contribution of FRP bars in the load and moment capacities. In addition, a parametric study was conducted to investigate the influence of the compressive strength of the GPC, longitudinal reinforcement ratio and confinement ratio on the *P-M* interaction behavior of the column. The developed analytical model conservatively predicted the *P-M* interaction behavior of the column. It was found that the compressive strength of the GPC, the longitudinal reinforcement ratio and the confinement ratio significantly influenced the *P-M* interaction behavior of the column. All the tested parameters resulted in the linear increase of load and moment capacities with the increase in the tested parameter.

Keywords: Columns; analytical model; Geopolymer concrete; FRP reinforcement; FRP tube; *P-M* interaction.

1. Introduction

Concrete is a widely utilized material in the construction industry around the globe [1]. With an increase in the development of the infrastructure across the world, the utilization of concrete is also increasing [2]. The annual global utilization of concrete is estimated to be approximately ten billion tons [3]. The Ordinary Portland cement (OPC) is a primary component of conventional concrete. The manufacturing process of OPC contributes to the overall carbon dioxide (CO_2) emissions in the atmosphere [4]. The CO_2 emission leads to global warming, which is recognized as a threat to the sustainable development of the world [5]. Approximately,

one ton of OPC manufacturing results in one ton of CO_2 emission [6]. Also, the overall manufacturing of OPC contributes to 5% to 7% of the annual CO_2 emissions globally [7].

Geopolymer concrete (GPC) was developed in an attempt to replace the OPC concrete (OPCC) and reduce the environmental impacts cuased by the construction industry [8-10]. Geopolymer concrete can be prepared by the fusion of alumina-silicate binders with the alkaline activator. Also, the industrial wastes or by-products, including fly ash (FA) and ground granulated blast furnace slag (GGBFS), can be utilized in the production of GPC [11-13]. Considering GPC as green concrete, research studies around the world are focused on exploring the new avenues of practical applications of GPC in structural members [14, 15].

The durability of steel reinforced concrete (RC) columns is a major concern due to the susceptibility of the corrosion of steel reinforcement in aggressive environments [16]. Fiber reinforced polymer (FRP) reinforcement was developed with a motive to address the durability issues of RC structures by replacing steel reinforcement with FRP reinforcement. The FRP reinforcement exhibits higher corrosion resistance, higher tensile strength, and lower weight than the equivalent steel reinforcement [17, 18]. Several studies explored the behavior of the FRP reinforcing bars in OPCC and GPC columns [19-23]. The mechanical properties of FRP reinforcement differ than that of the steel reinforcement. Higher tensile strength and lower elastic modulus are obtained by the FRP reinforcement than the steel reinforcement [24]. The difference in the mechanical properties results in the variance in the behavior of steel reinforced and FRP bars reinforced concrete columns.

Concrete filled FRP tube (CFFT) columns have arisen as an attractive alternative to the steel bar RC columns [25]. The GPC and high strength concrete (HSC) are considered brittle concrete [26, 27]. The use of CFFT enhances the ultimate concrete compressive strain, which improves the ductility of GPC and other HSC [26]. In addition, the use of CFFT offers added

advantages, including the use of left-in-place formwork and ease in the construction of columns. Moreover, CFFT columns exhibit higher strength and ductility than the steel bar RC columns [25, 28]. Hadi et al. [29] investigated the behavior of GPC filled basalt FRP (BFRP) tube circular column internally reinforced with BFRP bars. Hadi et al. [29] highlighted that the BFRP reinforced GPC filled BFRP tube column was a suitable alternative to the steel bar reinforced OPCC column with high corrosion resistance and ductility, contributing to the development of sustainable infrastructure. The use of GPC, BFRP bars and BFRP tube in place of OPCC, steel bars and steel helices, respectively, increased the sustainability, corrosion resistance and ductility of the column.

Columns are primarily designed to resist axial compressive loads. However, in practice, columns may experience the combination of axial compressive load and moments. The moments may be produced as a result of vertical misalignment or geometric imperfections or the position of the column in the structure [30]. The combination of axial and flexural loads on a column influences the compressive behavior of the column and thus requires investigation. However, a limited number of research studies were conducted on the load-moment (*P-M*) interaction behavior of CFFT circular columns internally reinforced with FRP bars [31-33]. These studies presented the methodology to develop the *P-M* interaction behavior of FRP reinforced OPCC filled FRP tube columns. Recent studies on FRP confined GPC conducted by Ozbakkaloglu and Xie [34], Lokuge and Karunasena [35] and Ahmad et al. [36] concluded that the behavior of FRP confined GPC was different from the behavior of FRP confined OPCC. Hence, it is significantly important to investigate the *P-M* interaction behavior of the FRP reinforced GPC filled FRP tube columns for its wide practical applications.

The *P-M* interaction behavior of the FRP reinforced GPC filled FRP tube circular column has not been explored in the available literature. Also, investigations are required to understand the influence of different parameters on the *P-M* interaction behavior of the GPC filled FRP tube

circular columns internally reinforced with FRP bars. Hence, the aim of this research study is to present a procedure for the development of the *P-M* interaction behavior of the steel reinforced GPC circular columns and FRP reinforced geopolymer concrete filled FRP tube circular columns for developing future design guidelines. The proposed analytical approach was developed, adopting the layer-by-layer numerical integration method. The analytical results were validated against the results of the experimental study conducted by Hadi et al. [29] and Ahmad et al. [37]. Also, a parametric study was conducted to ascertain the effect of compressive strength of GPC and the ratio of longitudinal reinforcement on the *P-M* interaction behavior of the FRP reinforced GPC filled FRP tube column.

2. Analytical modeling

2.1 Modeling of steel reinforced GPC

The concrete in the steel reinforced GPC circular columns was modeled as unconfined concrete, ignoring the contribution of steel helices. This is because the contribution of steel helices in confining the concrete up to the yielding of steel reinforcement is very limited. Hence, the contribution of the steel helices is ignored in the calculation of load and moment capacity of the columns [38].

2.1.1 Modeling of unconfined GPC

The GPC in the steel reinforced GPC columns was modeled based on the stress-strain model of GPC presented by Sarker [39]. The model is presented in Eqs. (1) and (2). The same model was also used by Farhan et al. [40] for steel reinforced GPC.

$$\frac{f_c}{f'_{co}} = \frac{zn}{n - 1 + z^{nk}} \tag{1}$$

$$z = \frac{\varepsilon_c}{\varepsilon_{co}} \tag{2}$$

where f_c and ε_c are the stress and strain, respectively, at any point on the stress-strain curve; f_{co}' and ε_{co} are the unconfined concrete compressive strength and corresponding strain, respectively, as defined in ACI 440.2R-17 [41]; n and k are the curve fitting factor and shape factor, respectively, which control the shape of ascending and descending segments of the stress-strain curve. The factor n was calculated using Eq. (3), as suggested in Sarker [39].

$$n = 0.8 + \frac{f_{co}'}{12} \tag{3}$$

The strain at unconfined concrete strength (ε_{co}) and k were calculated as per Collins and Mitchell [42] and expressed by Eq. (4) to Eq. (6).

$$\varepsilon_{co} = \left(\frac{n}{n-1}\right)\left(\frac{f_{co}'}{E_c}\right) \tag{4}$$

$$k = 1 \quad for \quad z \leq 1 \tag{5}$$

$$k = 0.67 + \frac{f_{co}'}{62} \quad for \quad z > 1 \tag{6}$$

The recommendation in Hardjito et al. [43] was used for the calculation of the modulus of elasticity of GPC (Eq. 7).

$$E_{GPC} = 2707\sqrt{f_{co}'} + 5300 \quad \text{(MPa)} \tag{7}$$

2.1.2 Modeling of steel reinforcement

The stress in the steel bar (f_s) was determined using the elastic modulus and the strain in the steel bar (ε_s), as presented in Eq. (8). It is noted that the relationship shown in Eq. (8) is based on the elastic perfectly plastic behavior of the steel bar.

$$f_s = E_s\varepsilon_s \ \leq \ f_y \tag{8}$$

where f_y and E_s are the yield stress and the elastic modulus of the steel bar, respectively.

2.2 Modeling of FRP reinforced GPC filled FRP tube columns

The GPC in the FRP reinforced GPC filled FRP tube circular columns was modeled as the confined geopolymer concrete.

2.2.1 Modeling of confined GPC

The stress-strain model for FRP confined GPC is not available in the literature. Ahmad et al. [36] tested FRP confined GPC and compared the test results with different confinement models available for FRP confined OPCC. Ahmad et al. [36] reported that the model presented in Youssef et al. [44] for FRP confined OPCC was able to predict the peak compressive stress and corresponding strain of FRP confined GPC with the least average absolute error. Also, the stress-strain curve of the FRP confined GPC developed using Youssef et al. [44] model was close to the experimental stress-strain curve of the FRP confined GPC. Thus, the model suggested in Youssef et al. [44] with a few modifications was adopted in this study for modeling the behavior of FRP confined GPC. One of the modifications was replacing the elastic modulus of OPCC with the elastic modulus of GPC, which was determined using Eq. (7). Also, Lam and Teng [45] observed that the use of actual maximum confinement pressure of the FRP confinement could result in better prediction of confined concrete behavior, as compared to the use of maximum confinement pressure. The actual maximum confinement pressure is based on the hoop rupture strain of the FRP confinement. The maximum confinement pressure provided by the FRP tube in the model proposed by Youssef et al. [44] was replaced with the actual maximum confinement pressure, which can be calculated based on the recommendation in ACI 440.2R-17 [41].

Youssef et al. [44] presented the stress-strain model for FRP confined OPCC with two branches and is expressed by Eqs. (9) and (10).

$$f_c = \varepsilon_c E_{GPC}\left[1 - \frac{1}{n'}\left(1 - \frac{E_2}{E_{GPC}}\right)\left(\frac{\varepsilon_c}{\varepsilon_t}\right)^{n'-1}\right] \quad \text{for} \quad 0 \le \varepsilon_c \le \varepsilon_t \tag{9}$$

$$f_c = f_t + E_2(\varepsilon_c - \varepsilon_t) \quad \text{for} \quad \varepsilon_t \le \varepsilon_c \le \varepsilon_{cu} \tag{10}$$

where f_c, ε_c, E_{GPC} and E_2 are the stress at any point of confined GPC, strain at any point of confined GPC, modulus of elasticity of GPC determined from Eq. (7) and slope of the second branch of the stress-strain curve, respectively. The stress and strain at the transition point between the two branches of the stress-strain curve are denoted by f_t and ε_t, respectively. The factor n' is the curve fitting factor and can be determined from Eq. (11).

$$n' = \frac{(E_{GPC} - E_2)\varepsilon_t}{E_{GPC}\varepsilon_t - f_t} \tag{11}$$

The stress and strain at the transition point can be determined using Eqs. (12) and (13), respectively.

$$f_t = f'_{co} + 3f'_{co}\left(\frac{\rho_{frp}E_{frp}\varepsilon_{tfrp}}{f'_{co}}\right)^{1.25} \tag{12}$$

$$\varepsilon_t = 0.002748 + 0.1169\left(\frac{\rho_{frp}E_{frp}\varepsilon_{tfrp}}{f'_{co}}\right)^{\frac{6}{7}}\left(\frac{f_{frp}}{E_{frp}}\right)^{\frac{1}{2}} \tag{13}$$

where f_{frp}, ρ_{frp} and ε_{tfrp} are the ultimate tensile stress of the FRP tube in the circumferential direction as determined from the material tests, volumetric ratio of the FRP tube confinement and strain in the FRP tube at the transition point, respectively. The volumetric ratio of FRP tube confinement can be determined using Eq. (14).

$$\rho_{frp} = \frac{4t}{D} \tag{14}$$

where t is the thicknes and D is the diameter of the FRP tube, respectively. The strain in the FRP tube at the transition point (ε_{tfrp}) was considered 0.002, as suggested by Youssef et al. [44]. The slope of the second branch of the stress-strain curve can be determined using Eq. (15).

$$E_2 = \frac{f'_{cc} - f'_{co}}{\varepsilon_{cu} - \varepsilon_t} \tag{15}$$

The ultimate compressive stress (f_{cc}') and ultimate compressive strain (ε_{cu}) conditions of the FRP confined GPC were determined with the relationships presented in Eqs. (16) and (17), respectively.

$$f_{cc}' = f_{co}' + 2.25 f_{co}' \left(\frac{f_{l,a}}{f_{co}'}\right)^{1.25} \tag{16}$$

$$\varepsilon_{cu} = 0.003368 + 0.2590 \left(\frac{f_{l,a}}{f_{co}'}\right)\left(\frac{f_{frp}}{E_{frp}}\right)^{0.5} \tag{17}$$

where $f_{l,a}$ is the actual confinement pressure, which can be determined using Eq. (18), as recommended in ACI 440.2R-17 [41].

$$f_{l,a} = \frac{2E_{frp} t \varepsilon_{h,rup}}{D} \tag{18}$$

$$\varepsilon_{h,rup} = k_{\varepsilon} \varepsilon_{frp} \tag{19}$$

where $\varepsilon_{h,rup}$ is the rupture strain of FRP tube in the circumferential direction, which can be determined by using Eq. (19). In Eq. (19), ε_{frp} is the ultimate tensile strain of the FRP tube in the circumferential direction and k_{ε} is the FRP strain efficiency factor, as defined in ACI 440.2R-17 [41]. A value of 0.55 was used for the FRP strain efficiency factor, as recommended in ACI 440.2R-17 [41].

2.2.2 Modeling of FRP bars

The stress in the FRP reinforcing bar (f_b) at a particular strain (ε_b) was determined as a function of the elastic modulus of the FRP bar (E_b). The relationship between stress and strain of the FRP bar is linear elastic until the rupture of FRP bar and is expressed as Eq. (20).

$$f_b = E_b \varepsilon_b \tag{20}$$

3. Analytical load moment interactions

Based on the presented material models, an analytical model for the *P-M* interaction diagram of FRP reinforced GPC filled FRP tube column was developed. The development of the analytical model for the *P-M* interaction diagram has been briefly discussed below.

3.1 Columns under concentric load

The first point on a *P-M* interaction diagram is on the load axis representing the column under concentric axial load. The axial load capacity (P_{ns}) of the steel reinforced GPC column was calculated using Eq. (21), as suggested in ACI 318-19 [38]. A similar expression was also used for modelling the steel reinforced geopolymer concrete columns in Farhan et al. [40]

$$P_{ns} = \alpha f_c'\left(A_g - A_s\right) + f_y A_s \tag{21}$$

where α is the strength reduction factor; f_c' is the average compressive strength of concrete at 28 days; f_y is the yield strength of steel; A_g represents the gross cross-sectional area of the column; A_s refers to the cross-sectional area of steel bars, respectively. The axial load capacity (P_{nb}) of FRP reinforced GPC filled FRP tube columns was calculated using Eq. (22), developed based on the recommendations in Maranan et al. [22]. Maranan et al. [22] found that the contribution of FRP bars by considering the elastic modulus and failure strain of FRP bars resulted in the most accurate predictions for the nominal capacity of the FRP reinforced GPC columns. However, the equation proposed by Maranan et al. [22] did not account for the FRP tube confinement. Therefore, the equation proposed by Maranan et al. [22] has been modified as Eq. (22) to account for the confined GPC strength in addition to the FRP bars contribution in the load carrying capacity of the FRP reinforced GPC filled FRP tube columns.

$$P_{nb} = \alpha f_{cc}'\left(A_g - A_b\right) + E_b \varepsilon_f A_b \tag{22}$$

where A_b is the cross-sectional area of FRP bars and ε_f is the strain in the FRP bar at failure. It was assumed that the bond between the FRP bar and surrounding GPC is perfect. A similar

assumption was made in several research studies [20, 24, 33]. Therefore, the strain in the FRP bar at the failure of the column was considered to be equal to ε_{cu} for the FRP reinforced GPC filled FRP tube columns. The strength reduction factor (α) of 0.85 has been adopted in numerous research studies on OPCC columns [20, 31, 32]. However, Maranan et al. [22] recommended that the strength reduction factor for GPC should be higher than the strength reduction factor for OPCC. Hence, the strength reduction factor for GPCC was considered as 0.9, based on the recommendation in Maranan et al. [22].

3.2 Columns under eccentric and flexural load

The load and moment capacity of the columns under eccentric and pure bending loads were determined using the layer-by-layer numerical integration method. This method has been used in several research studies for the development of *P-M* interaction curves [24, 31, 33, 40]. The feasibility of this method to investigate the *P-M* interaction behavior of the FRP tube confined FRP reinforced GPC has not been assessed yet. In this method, the cross-section of the column was assumed to consist of *m* horizontal layers, as shown in Fig. 1. The accuracy of the result increases with the reduction in the thickness of the layer. Thus, in this study, the thickness of each layer was assumed to be 1 mm. Figures 1(a) and 1(b) show the strain, stress and force distribution along the cross-section of steel reinforced GPC column and FRP reinforced GPC filled FRP tube column, respectively. The following assumptions were made for developing the analytical procedure.

a. A plane section remains plane before and after bending.

b. The strain distribution along the cross-section of the column is linear.

c. The strain in a single layer is uniform.

d. The tensile strength of GPC is ignored, as the tensile strength of GPC is significantly lower than its compressive strength.

e. The compressive strength of FRP tube is ignored, as the majority of the fibers in the tube were oriented in the hoop direction and did not contribute to the strength in the longitudinal direction.

f. The bond between steel or FRP bars and surrounding GPC is perfect.

g. The composite action between the FRP tube and GPC is fully developed.

A neutral axis depth (c) was assumed to start the procedure. The strain at the center of each layer can be determined using Eq. (23).

$$\varepsilon_{ci} = \left[\frac{c - \left(i - \frac{1}{2}\right) t_i}{c}\right] \varepsilon_{cu} \tag{23}$$

where i is the number of the layer from extreme compression face, t_i is the thickness of the layer and ε_{cu} is the ultimate concrete strain at the extreme compression face. The value of ε_{cu} was used as 0.003 for steel reinforced unconfined GPC columns. Whereas for the FRP tube confined columns, ε_{cu} was calculated using Eq. (17). The stress (f_{ci}) in each layer of concrete for steel reinforced GPC columns was calculated using Eq. (1). The f_{ci} for confined GPC in case of tube confined columns was calculated using the stress-strain model presented in Eqs. (9) and (10). The force resulting in each concrete layer (F_{ci}) for steel bar reinforced GPC columns or FRP tube confined GPC columns was calculated using Eq. (24).

$$F_{ci} = f_{ci} A_i \tag{24}$$

where A_i is the area of concrete layer only, which was calculated by multiplying the thickness of the layer (1 mm in this study) with the average width (b_i). The average width (b_i) is the width of the concrete layer, excluding the external FRP tube, which was calculated using Eq. (25).

$$b_i = 2\sqrt{\left(\frac{D}{2}\right)^2 - \left\{\frac{D}{2} - \left(i - \frac{1}{2}\right)t_i\right\}^2} \quad (25)$$

where t_i refers to the thickness of the layer; D refers to the diameter of the infill concrete. The average width for FRP tube confined columns (b_o) was calculated using Eq. (25) by replacing D with D_o (outer diameter of FRP tube). For the FRP tube confined GPC columns, the tensile force due to the FRP tube at mid-height of each layer was determined using Eq. (26).

$$F_{ti} = E_{lfrp}\varepsilon_{ci}(A_o - A_i) \quad (26)$$

where E_{lfrp} is the elastic modulus of FRP tube in the longitudinal direction and A_o is the total area of the layer, including the concrete and the FRP tube, which was determined by multiplying the total width of the layer (b_o) with the thickness of the layer (t_i). The tensile force in the concrete was assumed to be zero for the layers under tension. Similarly, the compressive force (F_{ti}) in the FRP tube was assumed to be zero, where the layers were subjected to compressive strain. The strain in each reinforcing bar (either steel (ε_{si}) or FRP (ε_{bi})) was calculated using Eq. (27)

$$\varepsilon_i = \left[\frac{c - d_i}{c}\right]\varepsilon_{cu} \quad (27)$$

where d_i is the distance of the reinforcing bar from the extreme compression fiber. The stresses in each steel and FRP reinforcing bar were calculated using Eqs. (28) and (29), respectively.

$$f_{si} = E_s\varepsilon_{si} \leq f_y \quad (28)$$

$$f_{bi} = E_b\varepsilon_{bi} \leq f_{bu} \quad (29)$$

The forces in each steel bar (F_{si}) and FRP bar (F_{bi}) were determined using Eqs. (30) and (31), respectively.

$$F_{si} = f_{si}A_{si} \tag{30}$$

$$F_{bi} = f_{bi}A_{bi} \tag{31}$$

The areas of the longitudinal steel reinforcing bars and FRP reinforcing bars were taken into account in the calculation of forces of both the concrete and the reinforcement bars. Therefore, the contribution of the concrete area substituted by reinforcement bars was deducted from the load and moment capacities to avoid overestimation. The strain in concrete at the level of reinforcing bar (ε_{cdi}) was calculated using Eq. (27). The stress in the concrete (f_{cdi}) at the level of the respective reinforcing bar was calculated by replacing the respective strain (ε_{cdi}) in Eq. (1) for steel reinforcement and Eqs. (9) and (10) for FRP reinforcement. The compressive force and corresponding moment due to the concrete at the reinforcing bar area were calculated using Eq. (32) and Eq. (33), respectively.

$$F_{cdi} = f_{cdi}A_i \tag{32}$$

$$M_{cdi} = F_{cdi}\left(\frac{D}{2} - d_i\right) \tag{33}$$

where A_i is the area of the steel bar (A_{si}) or the FRP bar (A_{bi}) at any level, f_{cdi} is the stress at the level of the steel bar (f_{sdi}) or the FRP bar (f_{bdi}), F_{cdi} is the force in the area of concrete replaced by the steel bar (F_{sdi}) or the FRP bar (F_{bdi}), and M_{sdi} is the moment due to the area of concrete replaced by the steel bar (M_{sdi}) or FRP bar (M_{bdi}).

The eccentric load capacities of the steel reinforced GPC columns (P_{ns}) and FRP reinforced GPC filled FRP tube columns (P_{nb}) were determined using Eqs. (34) and (35), respectively.

$$P_{ns} = \sum(F_{ci} + F_{ti}) + \sum F_{si} - \sum F_{sdi} \tag{34}$$

$$P_{nb} = \sum (F_{ci} + F_{ti}) + \sum F_{bi} - \sum F_{bdi} \quad (35)$$

The moment capacities of the steel reinforced GPC columns (M_{ns}) and the FRP reinforced GPC filled FRP tube columns (M_{nb}) were calculated by using Eqs. (36) and (37), respectively.

$$M_{ns} = \sum (F_{ci}) \left\{ \frac{D}{2} - \left(i - \frac{1}{2} \right) t_i \right\} + \sum F_{si} \left(\frac{D}{2} - d_i \right) - \sum M_{sdi} \quad (36)$$

$$M_{nb} = \sum (F_{ci} + F_{ti}) \left\{ \frac{D_o}{2} - \left(i - \frac{1}{2} \right) t_i \right\} + \sum F_{bi} \left(\frac{D_o}{2} - d_i \right) - \sum M_{bdi} \quad (37)$$

The developed methodology was programmed in MS Excel to calculate the load and moment capacity at a particular eccentricity.

4. Validation of the developed methodology

4.1 Brief description of experimental results

The experimental program used to validate the developed methodology for the *P-M* interaction behavior of the FRP reinforced GPC filled FRP tube column consisted of twelve specimens. The experimental results and the details of the preparation, instrumentation and testing procedure have already been presented in Hadi et al. [29] and Ahmad et al. [37]. Table 1 shows the test matrix used in this study. The specimens were classified in three groups. The first group consisted of the steel reinforced GPC reference (R) columns with 200 mm diameter and 800 mm height. The steel reinforced specimens were reinforced longitudinally with 12 mm diameter steel bars and transversally with helices of 10 mm plain steel bar with 60 mm pitch. The second group included BFRP bar reinforced GPC filled BFRP tube columns (BGBT). The specimens in the second group were reinforced internally with 15 mm diameter longitudinal BFRP bars. The third group included glass FRP (GFRP) bar reinforced GPC filled GFRP tube columns (GGGT). The diameter of GFRP bars used for reinforcing the third group was 17 mm.

The internal diameter of both the GFRP and BFRP tubes was 200 mm with a thickness of 1.5 mm. The height of each tube column was 812 mm. Each group consists four specimens. One specimen from each group was subjected to pure concentric axial load. Two specimens of each group were subjected to eccentric axial loads: one under 25 mm and one under 50 mm eccentricity. The last specimen from each group was subjected to pure flexural load.

The average compressive strength of GPC at 28 days was 47 MPa determined by testing the cylinder of 153 mm diameter and 306 mm height. The steel and FRP bars were tested in tension in accordance with AS1391-07 [46] and ASTM D7205/D7205M-11 [47], respectively. The average tensile strength of steel, BFRP and GFRP bars was 650 MPa, 778 MPa and 749 MPa, respectively. The elastic modulus of BFRP and GFRP bars was 34.3 GPa and 36.8 GPa, respectively. The FRP bars were also tested in compression as per ASTM D695-15 [48]. The compressive strength of BFRP and GFRP bars was 517 MPa and 472 MPa, respectively. It can be observed that the tensile and compressive strength of BFRP bar is higher than the GFRP bar. However, the elastic modulus of BFRP bar is lower than the GFRP bar. The elastic modulus of the BFRP and GFRP tubes in the circumferential direction was 42.3 GPa and 57 GPa, respectively, tested in accordance with ASTM D2290-08 [49]. The details of the tests conducted to determine the mechanical properties of the materials can be found in Hadi et al. [29] and Ahmad et al. [37].

All the specimens were tested under concentric, eccentric and four-point bending loads. The experimental test setup, loading mechanism, detailed test results and discussion can be found in Hadi et al. [29] and Ahmad et al. [37]. It was observed that in the steel reinforced specimens, the failure started with the spalling of the concrete cover and was followed by the buckling of the longitudinal steel bars. The rupture of the steel helix and the crushing of the GPC resulted in the failure of the steel reinforced specimens. In the FRP reinforced GPC filled FRP tube columns, the failure initiated with the rupture of the internal FRP bars. Afterwards the

specimens experienced the complete failure with the rupture of the FRP tube. Experimental *P-M* interaction points were determined for all the specimens. The experimental load and moment values are shown in Table 2. The experimental *P-M* interactions were plotted in Fig. 2 for all three groups of specimens. For concentric and eccentric loaded specimens, the axial load was determined as the peak load resisted by each specimen. For eccentrically loaded specimens, the bending moment was determined using Eq. (38)

$$M = P(e) \tag{38}$$

where M, P and e are the moment capacity, peak load and eccentricity, respectively. For the specimens tested under flexural load, the moment was calculated using Eq. (39)

$$M = \frac{Pl}{6} \tag{39}$$

where P is the peak load experienced by the test specimen under flexural load and l is the span of the test specimen.

4.2 Comparison of experimental and analytical *P-M* interactions

Table 2 shows the experimental and analytical loads and moments for each tested specimen. The experimental *P-M* interaction points for all the three groups are compared with the analytical *P-M* interaction points in Fig. 2. It can be observed from Fig. 2(a) that for Group R, the stress-strain model presented in Sarker [39] provided reasonable correlations with the experimental *P-M* interaction diagram. For Specimens R-0, R-25 and R-50, the analytical axial loads calculated with the proposed model were 88%, 75% and 80% of the experimental loads, respectively. Also, the analytical moments calculated with the same model for Specimens R-25, R-50 and R-F were 76%, 80% and 78% of the experimental moments, respectively. The difference between the experimental and analytical results might be due to the assumptions made in this study. Although the contribution of the steel helices was ignored, the steel helices

might have provided some confinement in increasing the compressive strength of concrete, which might led to the difference in analytical and experimental capacities. It can be noticed from Fig. 2(a) that the analytical *P-M* interaction curve drawn with the developed model matched well with the experimental *P-M* interaction curve. This shows that the model developed in this study is conservative and can be used to design the steel reinforced GPC columns.

The comparison of the experimental and the analytical *P-M* interaction diagrams for Groups BGBT and GGGT is shown in Figs. 2(b) and 2(c), respectively. The analytical load capacity calculated with the proposed model for Specimens BGBT-0, BGBT-25, BGBT-50, GGGT-0, GGGT-25 and GGGT-50 was 91%, 95%, 106%, 80%, 87% and 91% of the experimental load capacity, respectively. This shows that the proposed model conservatively predicted the load capacity of all the specimens in both the groups except Specimen BGBT-50.

The analytical moment capacities calculated with the proposed model for Specimens BGBT-25, BGBT-50, BGBT-F, GGGT-25, GGGT-50 and GGGT-F were 95%, 106%, 99%, 87%, 91% and 99% of the experimental moment capacity, respectively. The load and moment capacities for Specimen BGBT-50 were overestimated by 6%. This might be due to the minor misalignment and increase in the load eccentricity, which caused the reduction in the experimental axial load and moment capacities. It is worth noting that because the material used for longitudinal and transverse reinforcement would affect the overall column performance, some differences in the column failure modes were anticipated during the experiments when the GFRP was used instead of BFRP. The brittleness of GFRP bars and tubes was higher than the birttleness of BFRP bars and tubes, respectively. The increased brittleness resulted in the earlier rupture of GFRP bars and tubes. This could have possibly resulted in the initiation of earlier failure of the GFRP reinforced columns as compared to the BFRP reinforced columns, which resulted in the lower accuracy for GFRP reinforced columns.

It can be noticed from Fig. 2(b) and Fig. 2(c) that the proposed model reasonably predicted the load and moment capacities of the FRP reinforced GPC filled FRP tube columns. Therefore, it can be deduced that the analytical procedure developed using the stress-strain model of Youssef et al. [44] can be used for the development of the *P-M* interaction behavior of FRP reinforced GPC filled FRP tube columns.

5. Parametric study

The developed analytical approach presented in this study was used to conduct a parametric study. The influence of the compressive strength of GPC (f_c'), longitudinal reinforcement ratio (ρ) and the confinement ratio (f_{la}/f_{co}) on the *P-M* interaction behavior of the FRP bar reinforced GPC filled FRP tube columns was investigated. All the other parameters, including cross-sectional dimension and height of the column, were used similar to those used in the experimental study.

5.1 Effect of the compressive strength of GPC

Six different compressive strengths of GPC (30, 40, 50, 60, 70 and 80 MPa) were used to ascertain the effect on the *P-M* interaction behavior of the FRP bar reinforced GPC filled FRP tube column. Figures 3(a) and 3(b) show the effect of the compressive strength of GPC on *P-M* interaction behavior of Groups BGBT and GGGT, respectively. As expected, the increase in the compressive strength of GPC led to an overall increase in the load and moment capacities of both groups. With the increase of f_c' of GPC from 30 MPa to 80 MPa, Groups BGBT and GGGT experienced an average increase of 58% in the concentric axial load carrying capacity and 13% in the pure bending moment capacity. Figure 4 and 5 show the variations of the load and moment capacities of the specimens, respectively, by increasing the compressive strength of GPC. It can be observed that the relationship of the load and moment capacities with the compressive strength of GPC is linear. Also, the slope of the curves in Fig. 4 and 5 shows that

due to the increase in the compressive strength of GPC, the maximum increase was observed in the concentric load capacity of the specimens, and the minimum increase was observed in the moment capacity of the specimens tested in four-point bending. It can be attributed to the fact that the compressive strength of GPC has a dominant role in the axial load carrying capacity of the column as compared to the pure bending moment capacity of the column. Thus, the load and moment capacities of the FRP bar reinforced GPC filled FRP tube columns can be significantly improved with the use of high strength GPC.

5.2 Effect of the longitudinal reinforcement ratio

The longitudinal reinforcement ratio (ρ) is one of the main parameters in the *P-M* interaction behavior of the proposed column type. The minimum and maximum limits of the longitudinal reinforcement ratio in a column as per ACI 318-19 [38] are 1% and 8%, respectively. Five different longitudinal reinforcement ratios (1.45%, 2.46%, 3.27%, 5.25% and 7.05%) for different FRP bar sizes (10 mm, 13 mm, 15 mm, 19 mm and 22 mm) were used to conduct the parametric study. The longitudinal reinforcement ratios were varied while keeping all the other parameters constant. A similar approach was adopted to study the effect of longitudinal reinforcement ratio on the *P-M* interaction curve in several research studies [20, 24, 31, 32, 40]. The influence of the longitudinal reinforcement ratio on the *P-M* interaction behavior of Group BGBT and GGGT is shown in Figs. 6(a) and 6(b), respectively. It can be observed that Groups BGBT and GGGT experienced an average increase of 31% in the concentric load capacity and 41% in the pure bending capacity when the ρ was increased from 1.45% to 7.05%. Figures 7 and 8 show the variation of the load and moment capacities of the specimens, respectively, with the increase in the reinforcement ratio. It can be observed that the relationship of the reinforcement ratio with the load and moment capacities is linear. The enhancement of pure bending capacity with the increase of the reinforcement ratio was significant. This is because, under pure bending conditions, the internal FRP bars were in

tension and the tensile strength of FRP bar is higher than its compressive strength. In addition, it can be noticed that with the increase in ρ, Groups BGBT and GGGT showed almost a similar increase in the load and moment capacities of both the groups.

5.3 Effect of the confinement ratio

The confinement ratio (f_{la}/f_{co}) also influences the load and moment capacities of the confined specimens. Five different confinement ratios (0.1, 0.15, 0.2, 0.25 and 0.3) were used to ascertain its effect on the *P-M* interaction behavior of the FRP bar reinforced GPC filled FRP tube columns. The confinement ratios were selected to satisfy the condition of minimum confinement ratio for developing a strain hardening response. The ACI 440.2R-17 [41] recommended a minimum confinement ratio of 0.08 to assure a non-descending second branch of the stress-strain curve. The confinement ratios were varied while keeping all the other parameters constant. The influence of the confinement ratio on the *P-M* interaction behavior of Group BGBT and GGGT is shown in Figs. 9(a) and 9(b), respectively. It can be observed that Groups BGBT and GGGT experienced an average increase of 45% in the concentric load capacity and 57% in the pure bending capacity when the f_{la}/f_{co} increased from 0.1 to 0.3. Also, Fig. 10 and Fig. 11 show that the load and moment capacities of the specimens increased linearly with the increase in the confinement ratio. The increase in the load and moment capacities due to the increase in the confinement ratio is due to the increase in the confined concrete strength and confined concrete strain. The increase in confined concrete strain also led to the increase in the FRP bar strain and thus resulted in a higher increase in the bending capacity as compared to the concentric load capacity. A similar observation was reported by Karim et al. [50] for the GFRP reinforced columns confined with GFRP helices. It was also observed that both Groups BGBT and GGGT experienced almost a similar increase in *P-M* capacities with an equal increase in the confinement ratio. This shows that the behaviors of Group BGBT and GGGT are similar under low and high confinement pressures.

6. Conclusions

This study investigated the *P-M* interaction behavior of the GPC filled FRP tube columns internally reinforced with FRP bars. The layer-by-layer numerical integration approach was used. The theoretical approach was validated against the experimental results. In addition, a parametric study was carried out to understand the effects of the compressive strength of GPC and longitudinal reinforcement ratio on the *P-M* interaction behavior of the column. The conclusions deduced from the study are summarized as follows:

1. An analytical model was developed in this study to predict the *P-M* interaction behavior of the FRP reinforced GPC filled FRP tube columns. The developed model is capable of predicting the load and moment capacities of the FRP reinforced GPC filled FRP tube columns with a reasonable accuracy.

2. The increase of compressive strength of GPC from 30 MPa to 80 MPa resulted in an average increase of about 58% in the axial load capacity and 13% in pure bending capacity of the FRP reinforced GPC filled FRP tube columns.

3. The average increase in the moment capacities of the FRP reinforced GPC filled FRP tube columns was approximately 41%, with the increase of longitudinal reinforcement ratio from 1.45% to 7.05%. Also, the analytical investigation revealed that the increase in moment capacities for BFRP and GFRP reinforced specimens was similar for the increase of the same amount of longitudinal reinforcement.

4. The increase of confinement ratio from 0.1 to 0.3 resulted in an average increase of 45% in the load carrying capacity and 57% in the moment capacity of the FRP reinforced GPC filled FRP tube columns. The *P-M* behaviors of the BFRP and GFRP reinforced specimens were similar to each other under both low and high confinement pressures.

Acknowledgements

The authors acknowledge the help of technical officers Mr. Ritchie Mclean, Mr. Travis Marshall and Mr. Duncan Best for their help during the experimental phase of the study. Also, the first author would like to thank the University of Wollongong, Australia and Higher Education Commission (HEC) Pakistan for their joint PhD scholarship.

References

[1] Luhar S, Cheng TW, Luhar I. Incorporation of natural waste from agricultural and aquacultural farming as supplementary materials with green concrete: A review. Compos B Eng 2019;175:107076.

[2] Bellum RR, Muniraj K, Indukuri CSR, Madduru SRC. Investigation on Performance Enhancement of Fly ash-GGBFS Based Graphene Geopolymer Concrete. J Build Eng. 2020;32:101659.

[3] Arel HŞ, Aydin E. Use of industrial and agricultural wastes in construction concrete. ACI Mater J. 2018;115(1):55-64.

[4] Pasupathy K, Sanjayan J, Rajeev P. Evaluation of alkalinity changes and carbonation of geopolymer concrete exposed to wetting and drying. J Build Eng. 2020. 102029.

[5] Wong CL, Mo KH, Alengaram UJ, Yap SP. Mechanical strength and permeation properties of high calcium fly ash-based geopolymer containing recycled brick powder. J Build Eng. 2020;32:101655.

[6] Maries A, Hills CD, Carey P. Low-Carbon CO2-Activated Self-Pulverizing Cement for Sustainable Concrete Construction. J. Mater Civil Eng 2020;32(8):06020009.

[7] Gholampour A, Ho VD, Ozbakkaloglu T. Ambient-cured geopolymer mortars prepared with waste-based sands: Mechanical and durability-related properties and microstructure. Compos B Eng 2019;160:519-34.

[8] Davidovits J. Geopolymers and geopolymeric materials. J. Therm Anal 1989;35(2):429-41.

[9] Fan X, Zhou Z, Tu W, Zhang M. Shear behaviour of inorganic polymer concrete beams reinforced with basalt FRP bars and stirrups. Compos Struct. 2020;255:112901.

[10] Nawaz M, Heitor A, Sivakumar M. Geopolymers in construction-recent developments. Constr Build Mater. 2020;260:120472.

[11] Ali S, Sheikh MN, Sargeant M, Hadi MNS. Influence of Polypropylene and Glass Fibers on Alkali-Activated Slag/Fly Ash Concrete. ACI Struct J. 2020;117(4):183-92.

[12] Al-Hedad ASA, Farhan NA, Zhang M, Sheikh MN, Hadi MNS. Effect of geogrid reinforcement on the drying shrinkage and thermal expansion of geopolymer concrete. Struct Concrete 2020;21(3):1029-39.

[13] Verma M, Dev N. Sodium hydroxide effect on the mechanical properties of flyash-slag based geopolymer concrete. Struct Concrete 2020:1-12.

[14] Saranya P, Nagarajan P, Shashikala AP. Behaviour of GGBS-dolomite geopolymer concrete short column under axial loading. J Build Eng. 2020;30:101232.

[15] Shahmansouri AA, Bengar HA, Ghanbari S. Compressive strength prediction of eco-efficient GGBS-based geopolymer concrete using GEP method. J Build Eng. 2020:101326.

[16] Ali AH, Mohamed HM, Benmokrane B. Bar size effect on long-term durability of sand-coated basalt-FRP composite bars. Compos B Eng 2020;195:108059.

[17] AlAjarmeh OS, Manalo AC, Benmokrane B, Karunasena W, Mendis P. Effect of spiral spacing and concrete strength on behavior of GFRP-reinforced hollow concrete columns. J. Compos Constr 2020;24(1):04019054.

[18] Dong Z, Wu G, Xu B, Wang X, Taerwe L. Bond performance of alkaline solution pre-exposed FRP bars with concrete. Mag Concrete Res 2018;70(17):894-904.

[19] Hadi MNS, Karim H, Sheikh MN. Experimental Investigations on Circular Concrete Columns Reinforced with GFRP Bars and Helices under Different Loading Conditions. J. Compos Constr 2016;20(4):04016009.

514 [20] Salah-Eldin A, Mohamed HM, Benmokrane B. Axial–Flexural Performance of High-
515 Strength-Concrete Bridge Compression Members Reinforced with Basalt-FRP Bars and Ties:
516 Experimental and Theoretical Investigation. J. Bridge Eng 2019;24(7):04019069.
517 [21] Hasan HA, Sheikh MN, Hadi MNS. Performance evaluation of high strength concrete and
518 steel fibre high strength concrete columns reinforced with GFRP bars and helices. Constr Build
519 Mater 2017;134:297-310.
520 [22] Maranan GB, Manalo AC, Benmokrane B, Karunasena W, Mendis P. Behavior of
521 concentrically loaded geopolymer-concrete circular columns reinforced longitudinally and
522 transversely with GFRP bars. Eng Struct. 2016;117:422-36.
523 [23] Elchalakani M, Dong M, Karrech A, Li G, Ali MSM, Yang B. Experimental Investigation
524 of Rectangular Air-Cured Geopolymer Concrete Columns Reinforced with GFRP Bars and
525 Stirrups. J. Compos Constr. 2019;23(3):04019011.
526 [24] Hasan HA, Sheikh MN, Hadi MNS. Analytical investigation on the load-moment
527 characteristics of GFRP bar reinforced circular NSC and HSC columns. Constr Build Mater.
528 2018;183:605-17.
529 [25] Hadi MNS, Khan QS, Sheikh MN. Axial and flexural behavior of unreinforced and FRP
530 bar reinforced circular concrete filled FRP tube columns. Constr Build Mater. 2016;122:43-53.
531 [26] Ozbakkaloglu T, Vincent T. Axial Compressive Behavior of Circular High-Strength
532 Concrete-Filled FRP Tubes. J. Compos Constr. 2014;18(2):04013037.
533 [27] Pan Z, Sanjayan JG, Rangan BV. Fracture properties of geopolymer paste and concrete.
534 Mag Concrete Res. 2011;63(10):763-71.
535 [28] Abdallah MH, Mohamed HM, Masmoudi R. Experimental assessment and theoretical
536 evaluation of axial behavior of short and slender CFFT columns reinforced with steel and
537 CFRP bars. Constr Build Mater. 2018;181:535-50.

538 [29] Hadi MNS, Ahmad J, Yu T. Investigation of BFRP bar reinforced geopolymer concrete
539 filled BFRP tube columns. Proc. Inst Civil Eng - Struct Build. 2020:1-16.
540 [30] Lin G, Zeng JJ, Teng JG, Li LJ. Behavior of large-scale FRP-confined rectangular RC
541 columns under eccentric compression. Eng Struct. 2020;216:110759.
542 [31] Khan QS, Sheikh MN, Hadi MNS. Axial-flexural interactions of GFRP-CFFT columns
543 with and without reinforcing GFRP bars. J. Compos Constr. 2016;21(3):04016109.
544 [32] Khan QS, Sheikh MN, Hadi MNS. Concrete Filled Carbon FRP Tube (CFRP-CFFT)
545 columns with and without CFRP reinforcing bars: Axial-flexural interactions. Compos B Eng.
546 2018;133:42-52.
547 [33] Abdallah MH, Mohamed HM, Masmoudi R, Moussa A. Analytical modeling of moment-
548 curvature behavior of steel and CFRP RC circular confined columns. Compos Struct.
549 2018;189:473-87.
550 [34] Ozbakkaloglu T, Xie T. Geopolymer concrete-filled FRP tubes: Behavior of circular and
551 square columns under axial compression. Compos B Eng. 2016;96:215-30.
552 [35] Lokuge W, Karunasena W. Ductility enhancement of geopolymer concrete columns using
553 fibre-reinforced polymer confinement. J Compos Mater. 2015;50(14):1887-96.
554 [36] Ahmad J, Yu T, Hadi MNS. Basalt fiber reinforced polymer (BFRP) confined geopolymer
555 concrete. ACI Struct J. 2021; 118(1): 289-300.
556 [37] Ahmad J, Yu T, Hadi MNS. Experimental Investigations of GFRP bar reinforced
557 geopolymer concrete filled GFRP tube columns under different loading conditions. Structures.
558 2021; (under review).
559 [38] ACI 318-19. Building code requirements for structural concrete and commentary.
560 American Concrete Institute. Farmington Hills, MI. 2019.
561 [39] Sarker PK. Analysis of geopolymer concrete columns. Mater Struct. 2009;42(6):715-24.

562 [40] Farhan NA, Sheikh MN, Hadi MNS. Axial Load-Bending Moment (PM) Interactions of
563 Geopolymer Concrete Columns Reinforced with and without Steel Fiber. ACI Struct J.
564 2020;117(1):133-44.
565 [41] ACI 440.2R-17. Guide for the design and construction of externally bonded FRP systems
566 for strengthening concrete structures. ACI Committee 440, American Concrete Institute.
567 Farmington Hills, MI. 2017.
568 [42] Collins MP, Mitchell D. Prestressed concrete structures. Prentice Hall, Englewood Cliffs,
569 NJ. 1991.
570 [43] Hardjito D, Wallah S, Sumajouw D, Rangan B. The stress-strain behaviour of fly ash-
571 based geopolymer concrete. In: Developments in Mechanics of Structures and Materials. A A
572 Balkema Publishers, The Netherlands. 2004:831-34.
573 [44] Youssef MN, Feng MQ, Mosallam AS. Stress–strain model for concrete confined by FRP
574 composites. Compos B Eng. 2007;38(5-6):614-28.
575 [45] Lam L, Teng JG. Design-oriented stress-strain model for FRP confined concrete. Constr
576 Build Mater. 2003;17(6-7):471-89.
577 [46] AS 1391-07. Methods for tensile testing of metals. Standards Australia. 2007.
578 [47] ASTM D7205-11. Standard test method for tensile properties of fiber reinforced polymer
579 matrix composite bars. ASTM Internaional. West Conshohocken, PA. 2011.
580 [48] ASTM D695-15. Standard test method for compressive properties of rigid plastics. ASTM
581 Internaional. West Conshohocken, PA. 2015.
582 [49] ASTM D2290-08. Standard test method for apparent hoop tensile strength of plastic or
583 reinforced plastic pipe by split disk method. ASTM Internaional. West Conshohocken, PA.
584 2008.

585 [50] Karim H, Sheikh MN, Hadi MNS. Load and moment interaction diagram for circular
586 concrete columns reinforced with GFRP bars and GFRP helices. J. Compos. Constr.
587 2017:21(1);04016076.

Table 1: Test matrix

Group designation	Specimen designation	Longitudinal reinforcement	Lateral confinement	Loading eccentricity
R	R-0	Steel bars	Steel helix	0
	R-25			25
	R-50			50
	R-F			Flexure
BGBT	BGBT-0	BFRP bars	BFRP tube	0
	BGBT-25			25
	BGBT-50			50
	BGBT-F			Flexure
GGGT	GGGT-0	GFRP bars	GFRP tube	0
	GGGT-25			25
	GGGT-50			50
	GGGT-F			Flexure

Table 2: Experimental and analytical peak loads and moments

Specimen designation	Experimental		Analytical	
	Load (kN)	Moment (kN.m)	Load (kN)	Moment (kN.m)
R-0	1946	0	1707	0
R-25	1207	30	912	23
R-50	694	35	555	28
R-F	0	28	0	22
BGBT-0	1810	0	1649	0
BGBT-25	1159	29	1101	27
BGBT-50	660	33	704	35
BGBT-F	0	34	0	34
GGGT-0	2283	0	1822	0
GGGT-25	1354	34	1178	29
GGGT-50	826	41	753	38
GGGT-F	0	38	0	37

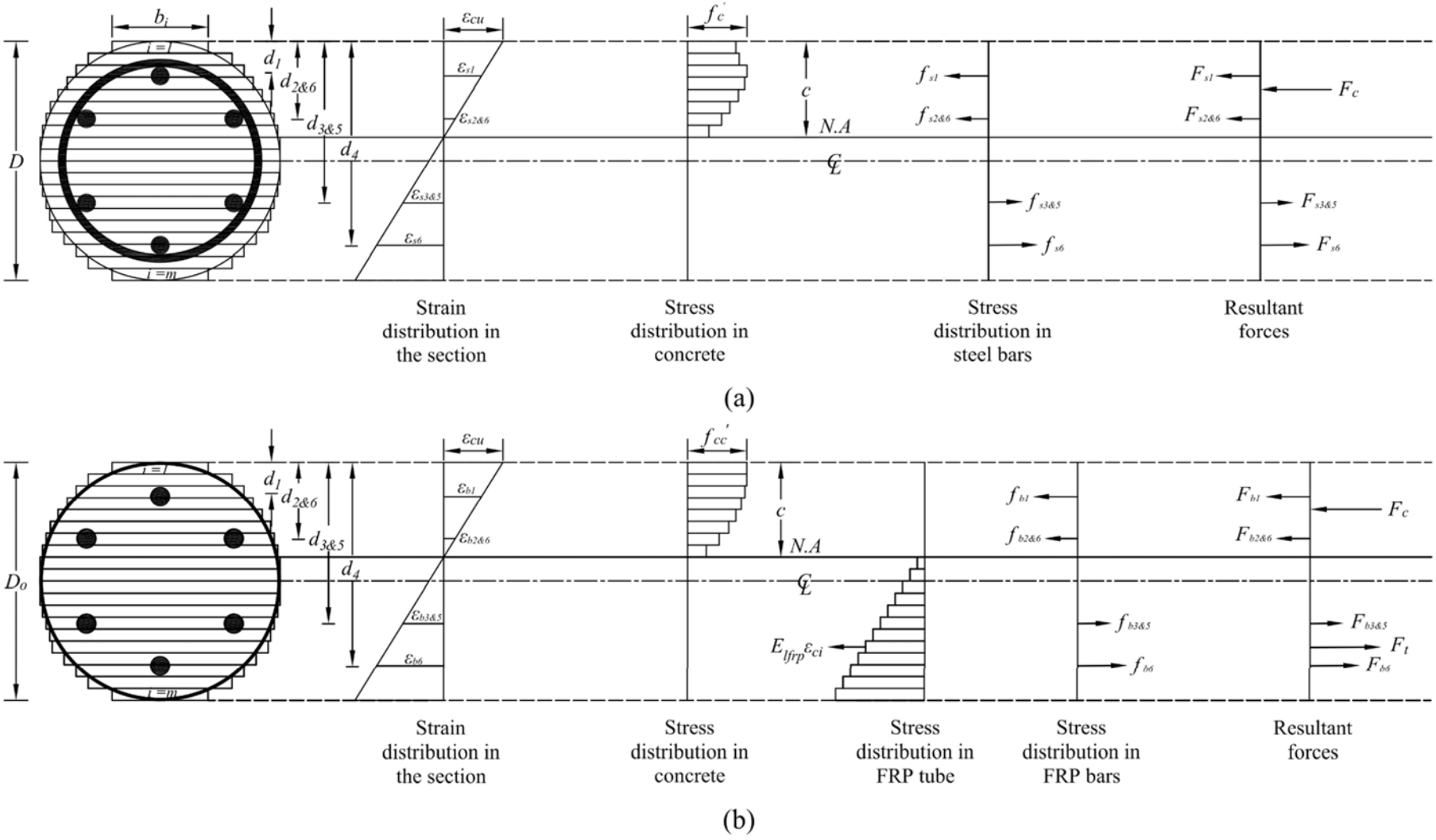

Fig. 1: Stress-strain distribution for the computation of *P-M* interactions of (a) steel reinforced GPC (b) FRP reinforced GPC filled FRP tube

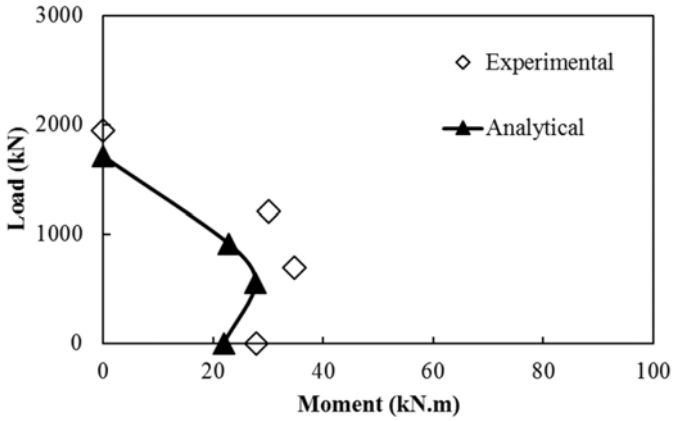

(a)

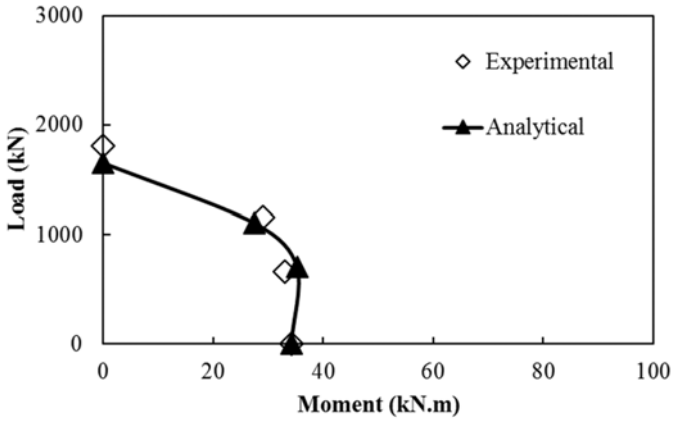

(b)

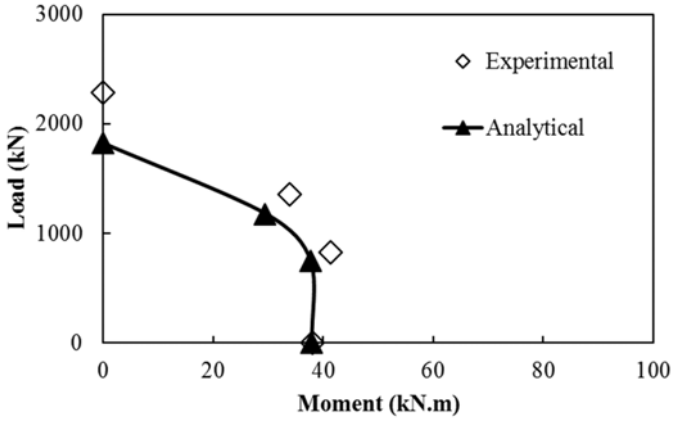

(c)

Fig. 2: Experimental and analytical *P*-*M* interaction diagrams of (a) Group R; (b) Group BGBT; (c) Group GGGT.

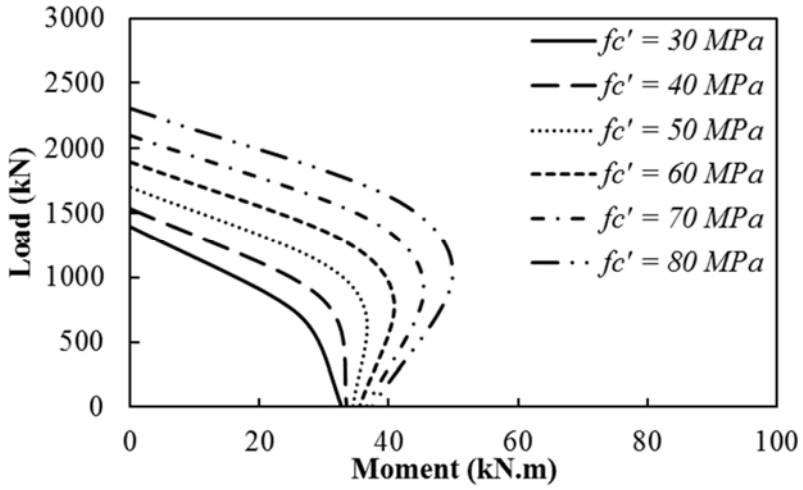

(a)

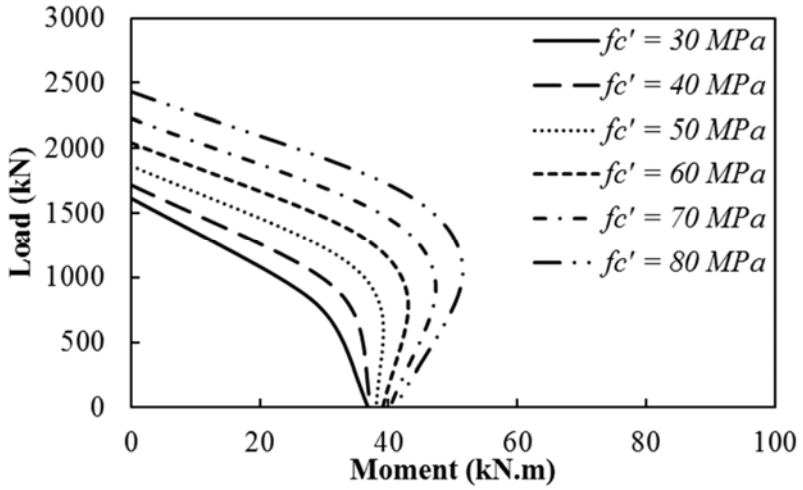

(b)

Fig. 3: Effect of compressive strength of GPC on *P-M* interaction curves for (a) Group BGBT and (b) Group GGGT

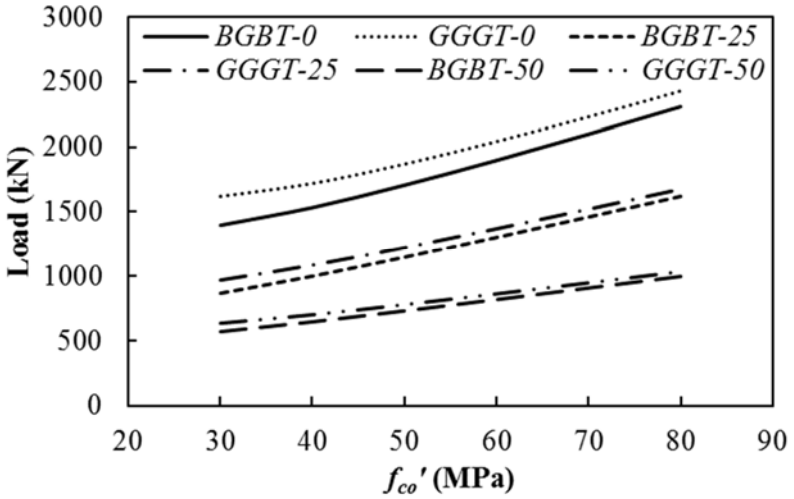

Fig. 4: Variation of the load carrying capacity of the specimens with the compressive strength of GPC

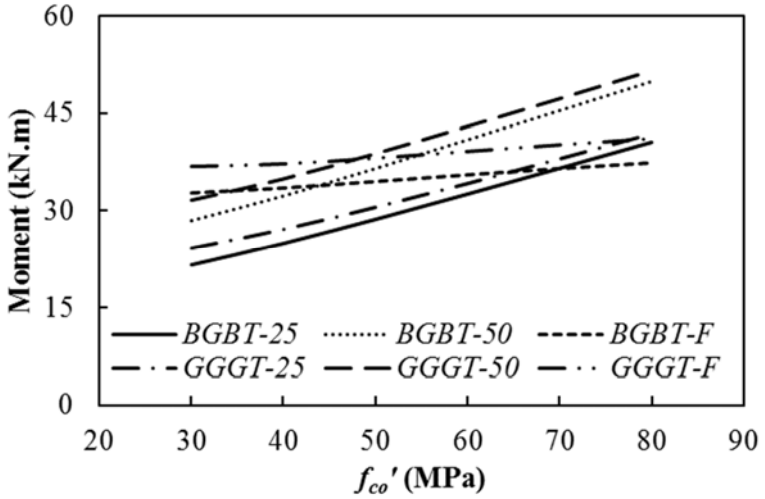

Fig. 5: Variation of the moment capacity of the specimens with the compressive strength of GPC

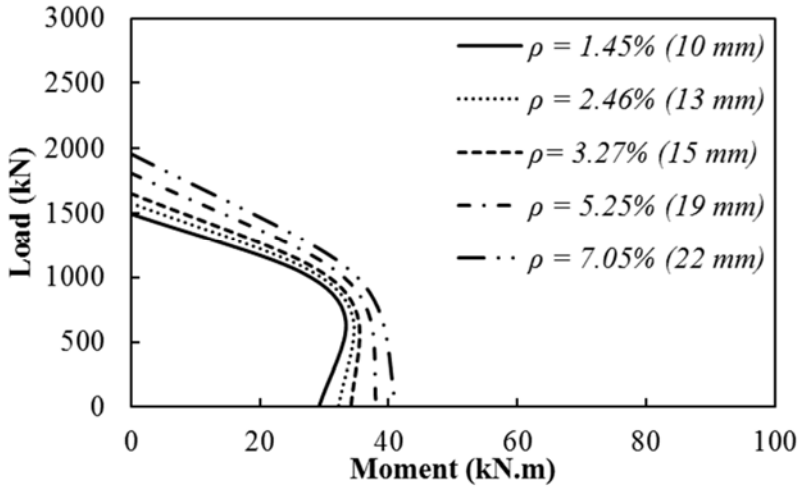

(a)

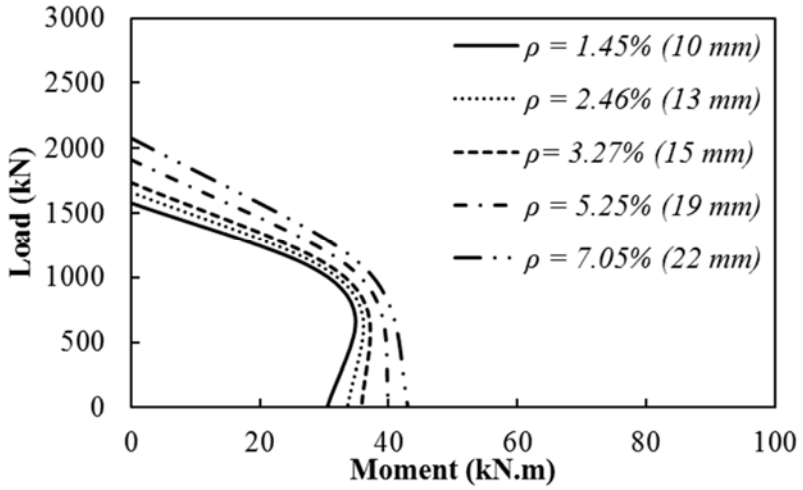

(b)

Fig. 6: Effect of longitudinal reinforcement ratio on *P-M* interaction curves for (a) Group BGBT and (b) Group GGGT

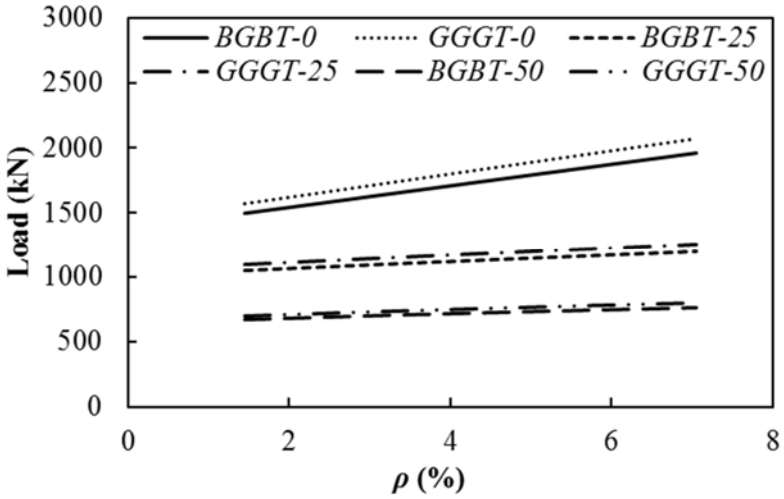

Fig. 7: Variation of the load carrying capacity of the specimens with the reinforcement ratio

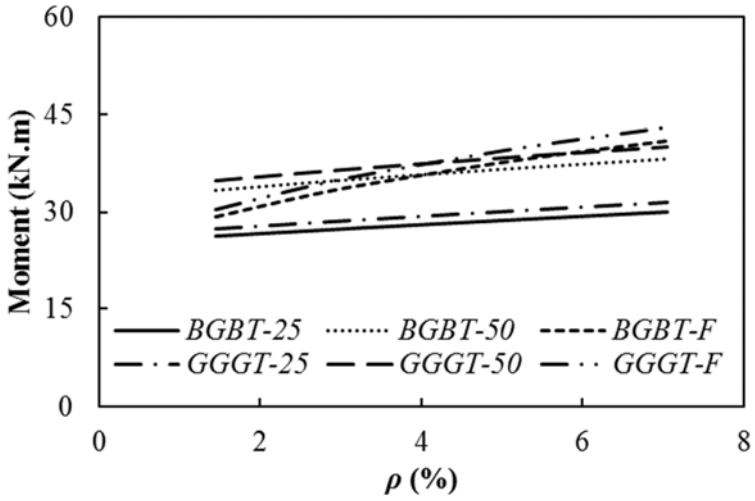

Fig. 8: Variation of the moment capacity of the specimens with the reinforcement ratio

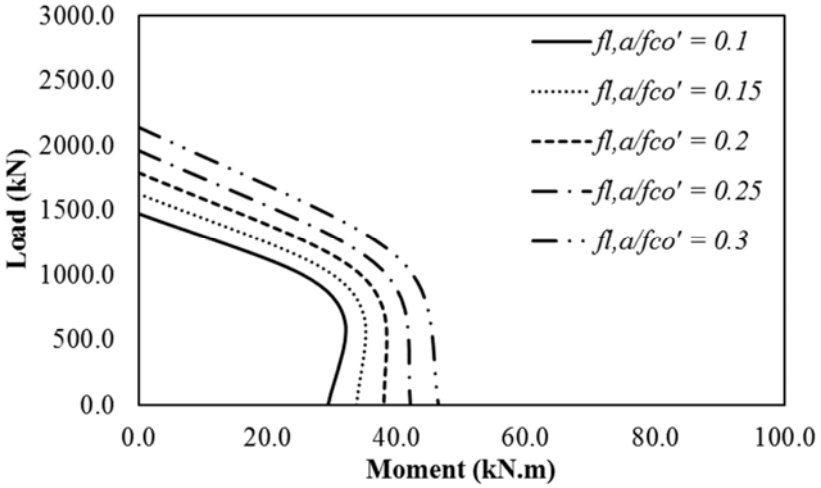

(a)

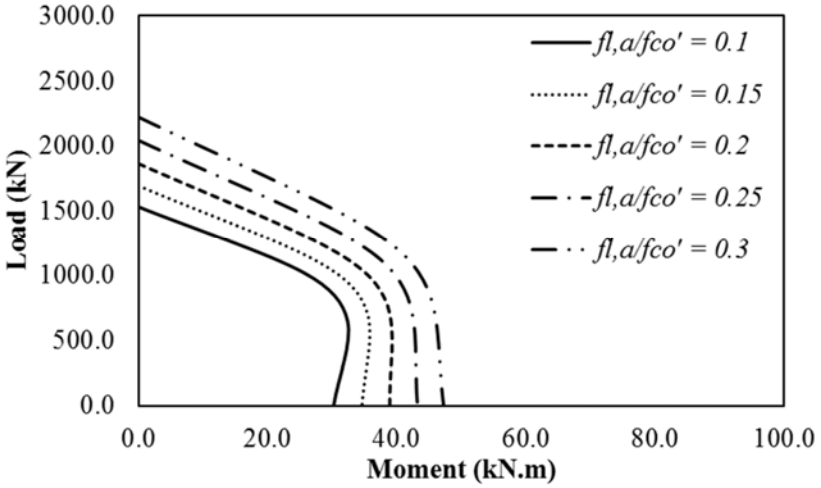

(b)

Fig. 9: Effect of confinement ratio on *P*-*M* interaction curves for (a) Group BGBT and (b) Group GGGT

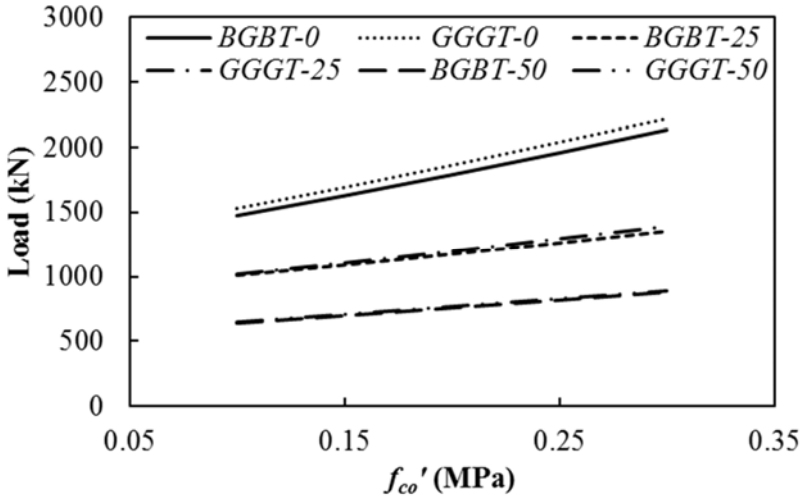

Fig. 10: Variation of the load carrying capacity of the specimens with the confinement ratio

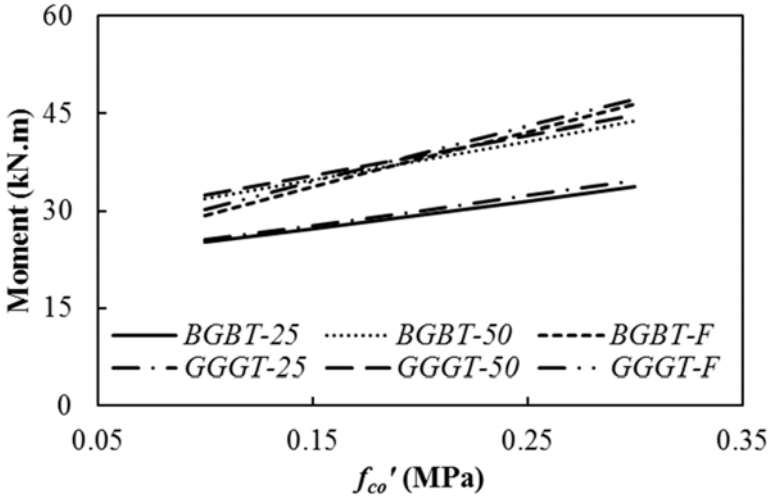

Fig. 11: Variation of the moment capacity of the specimens with the confinement ratio